

LARV: Data-Free Layer-wise Adaptive Rescaling Veneer for Model Merging

Xinyu Wang
University of Connecticut
xinyu.wang@uconn.edu

Ke Deng
University of Georgia
ke.deng@uga.edu

Fei Dou
University of Georgia
fei.dou@uga.edu

Jinbo Bi
University of Connecticut
jinbo.bi@uconn.edu

Jin Lu
University of Georgia
jin.lu@uga.edu

Abstract

Model merging aims to combine multiple fine-tuned models into a single multi-task model without access to training data. Existing task-vector merging methods such as TIES, TSV-M, and Iso-C/CTS differ in their aggregation rules but treat all layers nearly uniformly. This assumption overlooks the strong layer-wise heterogeneity in large vision transformers, where shallow layers are sensitive to interference while deeper layers encode stable task-specific features. We introduce LARV, a training-free, data-free, merger-agnostic **Layer-wise Adaptive Rescaling Veneer** that plugs into any task-vector merger and assigns a per-layer scale to each task vector before aggregation, and show it consistently boosts diverse merging rules. LARV adaptively suppresses shallow-layer interference and amplifies deeper-layer alignment using a simple deterministic schedule, requiring no retraining or modification to existing mergers. To our knowledge, this is the first work to perform layer-aware scaling for task-vector merging. LARV computes simple data-free layer proxies and turns them into scales through a lightweight rule; we study several instantiations within one framework (e.g., tiered two/three-level scaling with fixed values, or continuous mappings) and show that tiered choices offer the best robustness, while continuous mappings remain an ablation. LARV is orthogonal to the base merger and adds negligible cost. On FusionBench with Vision Transformers, LARV consistently improves all task-vector baselines across 8/14/20-task settings; for example, Iso-C + LARV reaches 85.9% on ViT-B/32, 89.2% on ViT-B/16, and 92.6% on ViT-L/14. Layer-wise analysis and corruption tests further indicate that LARV suppresses shallow-layer interference while modestly amplifying deeper, task-stable features, turning model merging into a robust, layer-aware procedure rather than a uniform one.

1. Introduction

Large pretrained vision models have made it practical to compose capabilities without retraining from scratch [1–3]. A convenient formalism is the task-vector view: a fine-tuned model for task i at layer ℓ can be written as $\theta_{i,\ell} = \theta_{0,\ell} + \Delta\theta_{i,\ell}$, where $\theta_{0,\ell}$ is the pretrained initializer and $\Delta\theta_{i,\ell}$ is a task-specific delta. Model merging combines a set of task vectors $\{\Delta\theta_{i,\ell}\}$ into one vector $\Delta\theta_\ell$ and then adds it to $\theta_{0,\ell}$, so the merged model inherits multiple skills while preserving the base model’s generality. This paradigm is both meaningful for revealing surprising linear structure in parameter space and useful for enabling capability sharing with no data, rapid deployment under data-access constraints, and mix-and-match assembly across tasks and architectures [4–8]. The ubiquity of weight averaging in practical distributed training further underscores its utility [9].

Despite rapid progress, most merging strategies make *global* choices that overlook depth [10]. Examples include a single mixing coefficient or checkpoint average [4], model-level importance weighting via curvature/Fisher information [5], and uniform, rule-based schemes aimed at reducing interference (e.g., sign consensus, trimming, or parameter reweighting) that act similarly across all layers [2, 7, 11, 12]. However, in deep networks this is a practical assumption: early layers predominantly encode high-frequency, local patterns that are information-dense yet fragile to noise and domain shift, whereas deeper layers tend to represent more semantic and stable features [13–16]. This fragility at shallow depth has been repeatedly observed under common corruptions and shortcut biases [17, 18]. When task vectors are combined without acknowledging this hierarchy, helpful updates in some layers can be weakened—or undone—by conflicting updates elsewhere, yielding unnecessary regressions [19].

This paper argues that merging should be layer-aware. Rather than treating every layer as equally trustworthy, we scale each layer’s contribution according to two properties:

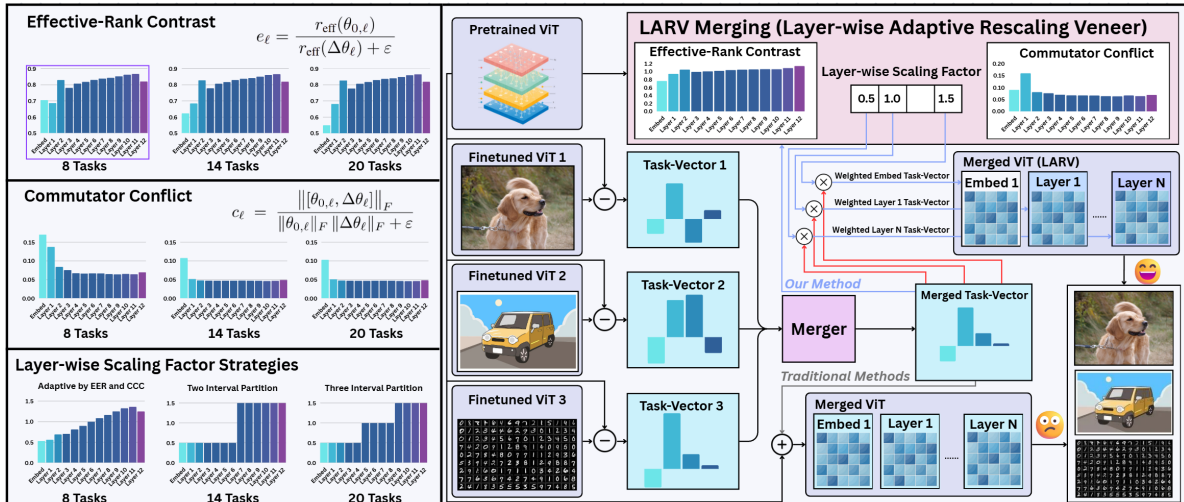


Figure 1. Overview of LARV merging. (Left) We compute two data-free, weight-derived diagnostics per layer—information richness e_ℓ and conflict level c_ℓ —which exhibit clear depth-dependent trends across 8/14/20-task merges. These signals are converted into layer-wise scaling factors via continuous or tiered mappings. (Right) Each task vector is rescaled at its corresponding layer and merged with any base rule, forming a lightweight veneer that suppresses shallow-layer interference while enhancing deeper-layer alignment.

(i) how much *information* the layer’s update appears to carry and (ii) how much *conflict* it exhibits with other task vectors. Crucially, our solution is data-free: it requires no examples, gradients, or feature statistics and can be used wherever task vectors are available.

We introduce LARV (Layer-wise Adaptive Rescaling Veneer), a simple add-on that rescales the merged delta per layer before it is added back to the pretrained model. Given any base merger that produces $\Delta\theta_{\text{merge},\ell}$ for each $\ell \in \{1, \dots, L\}$, LARV computes

$$\Delta\theta_{\text{larv},\ell} = r(e_\ell, c_\ell) \cdot \Delta\theta_\ell, \quad (1)$$

where $r(\cdot)$ is a scalar gate determined by two *data-free* diagnostics:

1. **Effective-Rank Contrast** (e_ℓ): a weight-only indicator of how structured and informative the update is at layer ℓ , with larger e_ℓ favoring concentrated, signal-bearing directions over diffuse noise.
2. **Commutator Conflict Coefficient** (c_ℓ): a measure of how strongly the update interferes with the base operator, where larger c_ℓ indicates greater non-commutativity and potential conflict.

Both quantities are computed directly from weights, with no data or gradients. Empirically, e_ℓ increases and c_ℓ decreases with depth, motivating a layer-wise schedule that down-weights fragile shallow layers and strengthens stable deeper layers [13, 14], yielding a lightweight veneer applicable to any task-vector merger.

Our contributions are threefold:

1. LARV is **compatible with essentially all task-vector merging methods**, highlighting that structural (depth-

aware) design matters and that layers should not share a single global scale.

2. We introduce novel indicators, e_ℓ (information richness) and c_ℓ (conflict level), to quantify per layer how much to encourage or discourage the merged update before recomposition, which yields a simple yet effective rule without acquiring data or gradients.
3. Across different base mergers and architectures, LARV yields consistent improvements as much as 7.7% on FusionBench [20], with detailed ablations, sensitivity analyses, and robustness evaluations to noise and distribution shift.

2. Related Work

Global and training-free merging. Early training-free methods merge parameters using *global* rules that largely ignore depth. Model Soups and weight averaging interpolate checkpoints without structural differentiation [4, 21]. Task Arithmetic treats the difference between a fine-tuned model and its pretrained ancestor as a task vector and composes vectors by addition or scaling [6]. Curvature-aware schemes such as Fisher-weighted averaging reweight parameters by importance but still apply a uniform rule across layers [5]. Regression Mean (RegMean) frames merging as a closed-form regression over layer inputs, again applying the same policy per layer [22]. Permutation-alignment works (e.g., Git Re-Basin, permutation-invariance analyses) are complementary. They improve compatibility among independently trained models prior to averaging [7, 8].

Structured and conflict-aware training-free merging. A second line adds structure to reduce interference while remaining training-free [23, 24]. TIES-Merging trims small deltas and enforces sign consistency to avoid destructive averaging [11]. DARE (Drop & Rescale) sparsifies task vectors by randomly resetting most delta parameters to base values and rescaling the remainder before merging [25]. EMR-Merging elects a unified task vector and attaches lightweight task-specific masks/rescalers applied at inference time [26]. TSV-M operates at the layer level, using singular vectors of per-layer task matrices to compress and whiten interference across tasks [27]. These methods demonstrate the utility of structural priors for dataless merging, yet most still apply a near-global policy to each layer’s update scale.

Adaptive or data-involving merging. Other approaches *learn* coefficients with auxiliary signals [28]. AdaMerging optimizes task-wise or layer-wise coefficients by entropy minimization on unlabeled test data, improving generalization under shift [29]. Twin-Merging learns routers to dynamically integrate shared and exclusive expertise across tasks [30]. Some recent conflict-aware designs (e.g., CAT-Merging) remain training-free but rely on parameter-type and devise specific trimming and projections rather than learned gates [23]. While these techniques increase flexibility, methods that learn coefficients typically require samples’ features and labels or considerable amount of extra compute at merge time.

Layer-wise representation studies and our position. A large body of work characterizes the *hierarchical* organization of deep networks: lower layers emphasize local/high-frequency patterns, while deeper layers encode more semantic and stable features [13–16]. Fragility at shallow depth under corruptions and shortcuts is well documented [17, 18]. Despite this, most mergers set a single global scale per model or per parameter type. LARV occupies the middle ground: it is *training-free* like global methods, yet explicitly layer-aware via two data-free diagnostics— e_ℓ (information richness) and c_ℓ (conflict level) that deterministically gate each layer’s update before recomposition. This yields interpretability and negligible overhead while capturing depth heterogeneity that global rules overlook.

3. Method

3.1. Preliminaries and Problem Setup

We consider a pretrained network θ_0 with L parametrized layers $\{\theta_{0,\ell}\}_{\ell=1}^L$. Each task $i \in \{1, \dots, K\}$ provides a *task vector* (delta) $\Delta\theta_i \triangleq \theta_i - \theta_0$ anchored at θ_0 , with layer-wise slices $\{\Delta\theta_{i,\ell}\}_{\ell=1}^L$. Task vectors may be full-rank updates or PEFT modules (adapters, LoRA, BitFit), which we fold into the ambient parameter space for merging [31–35]. A base

merger \mathcal{M} aggregates the per-layer deltas

$$\Delta\theta_\ell = \mathcal{M}(\{\Delta\theta_{i,\ell}\}_{i=1}^K), \quad \ell = 1, \dots, L, \quad (2)$$

where \mathcal{M} may be arithmetic/averaging (Model Soups, SWA) [4], curvature-aware (Fisher-weighted) [5], sign/trim-consistent (e.g., TIES-Merging) [11, 36], regression-style [22, 37], or permutation-aware alignment (Git Re-Basin, permutation invariance) [7, 8]. Classical training-free merging then injects $\Delta\theta_\ell$ using a *single global* coefficient s , as shown below in Eq. (3), implicitly assuming that all layers are equally trustworthy. Formally, we recall the standard uniform composition used throughout the merging literature:

$$\theta_{\text{merge},\ell} = \theta_{0,\ell} + s \cdot \Delta\theta_\ell, \quad (3)$$

where $s \in [0, \infty)$ controls the global blend (e.g., $s=1/K$ yields an even average for merging K models).

Eq. (3) treats every layer’s update equally, which is a convenient assumption; however, a global coefficient can be fragile [38]. A large body of empirical analysis shows that deep networks organize features hierarchically: earlier layers emphasize local/high-frequency patterns while later layers encode more semantic, task-relevant structure [13–16]. Consequently, a single scalar s *over-updates fragile early layers and under-updates decisive later layers*, even when \mathcal{M} is improved by curvature or sign heuristics. Permutation-aware methods [7, 8] mitigate *representational misalignment* but the application of the update remains uniform across depth. This motivates the layer-wise veneer we introduce next.

Why a single global scale is insufficient. Consider a minimal two-layer network $f(x) = W_2\phi(W_1x)$. Suppose two tasks A/B produce updates such that $\Delta W_1^A \approx -\Delta W_1^B$ (strong early-layer conflict) while $\Delta W_2^A \approx \Delta W_2^B$ (head agreement). Any global coefficient s scales both layers identically and therefore cannot suppress the conflicting layer-1 update while preserving the aligned layer-2 update; the optimum requires $s_1 \neq s_2$. This simple counterexample illustrates that uniform scaling cannot resolve depth-localized interference, motivating the need for layer-wise scaling.

3.2. LARV: Layer-wise Rescaling Veneer over Any Merger

Design goals. Given the insufficient treatment of depth-wise heterogeneity across depth, we seek a veneer that is *training-free* and *label-free*, (ii) is a merger-agnostic add-on that can wrap any base rule \mathcal{M} , and (iii) explicitly encodes *depth heterogeneity* consistent with representation studies [13–16].

Specifically, given the merged update $\Delta\theta_\ell$ at layer ℓ from Eq. (2), LARV’s goal is to compose a *layer-specific* scale:

$$\theta_{\text{merge},\ell} = \theta_{0,\ell} + s_\ell \cdot \Delta\theta_\ell, \quad \ell = 1, \dots, L, \quad (4)$$

where $s_\ell \in \mathbb{R}_{\geq 0}$ is chosen without any training or labels.

From weights alone, we compute two per-layer diagnostics: (i) an *information-richness* proxy e_ℓ (Effective-Rank Contrast ; see §3.2.1) and (ii) a *conflict* proxy c_ℓ (Commutator Conflict Coefficient). Then, based on the two diagnostics, a *composite weight-only score* is formulated by encouraging high information and penalizing conflict in the following subsection.

3.2.1. Weight-Only Metrics

Setup. As in §3.1, each parameterized module is viewed as a matrix: convolutions are folded into a $(\text{out} \times \text{in} \cdot k_h k_w)$ matrix; attention uses $Q/K/V/O$ projections as separate parameter groups for metric computation and averages their scores to one per-layer value. Biases and LayerNorm scale/shift are included in the final composition (Eq. (4)) but excluded from the spectral/commutator diagnostics to avoid degenerate shapes. We denote the base weights by $\theta_{0,\ell}$ and the merged update by $\Delta\theta_\ell$ (Eq. (2)).

(A) Effective-Rank Contrast (e_ℓ). Spectral entropy separates structured, low-rank updates from diffuse, noise-like ones. Let $\{\sigma_j(A)\}$ be the singular values of a matrix A ; define normalized energies $p_j(A) = \sigma_j(A)^2/\|A\|_F^2$ and spectral entropy $H(A) = -\sum_j p_j(A) \log p_j(A)$. The *effective rank* is $r_{\text{eff}}(A) = \exp(H(A))$, which is scale-invariant and larger for spectrally diffuse matrices. We compare the update to the base via a base-relative contrast:

$$e_\ell = \frac{r_{\text{eff}}(\theta_{0,\ell})}{r_{\text{eff}}(\Delta\theta_\ell) + \varepsilon}, \quad (5)$$

with a small $\varepsilon > 0$ for numerical stability. Thus e_ℓ is larger when $\Delta\theta_\ell$ is *more concentrated* (lower effective rank) than the base $\theta_{0,\ell}$, which is interpreted as a more informative, task-salient update, and it shrinks toward 0 when $\Delta\theta_\ell$ is as or more diffuse than the base.

We estimate $r_{\text{eff}}(\cdot)$ per layer using a lightweight randomized SVD (rank $k \in [32, 64]$), applied to each layer’s matrix view. This preserves the training-free nature and adds negligible overhead relative to a forward pass. (If $\|\Delta\theta_\ell\|_F$ is numerically zero, we set $e_\ell = 0$.)

This aligns with findings that deeper layers exhibit more semantic, low-intrinsic-dimension structure [15, 16]. As shown in the first column of Fig. 2, e_ℓ typically *increases* with depth on ViT backbones (see the first column in Fig. 2).

(B) Commutator Conflict Coefficient (c_ℓ). Order sensitivity (non-commutativity) between the base operator and the update acts like a rotation of features and signals potential interference. We quantify it by a scale-normalized commutator:

$$c_\ell = \frac{\|[\theta_{0,\ell}, \Delta\theta_\ell]\|_F}{\|\theta_{0,\ell}\|_F \|\Delta\theta_\ell\|_F + \varepsilon}, \quad (6)$$

with a small $\varepsilon > 0$ for numerical stability and we define the operator between two matrices as $[A, B] = AB - BA$. When $\theta_{0,\ell}$ and $\Delta\theta_\ell$ are rectangular, we use the average of left/right Gram-commutators (dimension-compatible and symmetric):

$$c_\ell = \frac{1}{2} \frac{\|\theta_{0,\ell} \Delta\theta_\ell^\top - \Delta\theta_\ell \theta_{0,\ell}^\top\|_F}{\|\theta_{0,\ell}\|_F \|\Delta\theta_\ell\|_F + \varepsilon} + \frac{1}{2} \frac{\|\theta_{0,\ell}^\top \Delta\theta_\ell - \Delta\theta_\ell^\top \theta_{0,\ell}\|_F}{\|\theta_{0,\ell}\|_F \|\Delta\theta_\ell\|_F + \varepsilon}. \quad (7)$$

This measures non-commutativity of the base operator and the update: if they commute, composition order doesn’t matter; if not, the update “rotates” features, indicating conflict. Large c_ℓ indicates destabilizing rotations and calls for shrinkage of the model update.

This quantity serves conceptually to measure commutativity and we will use it directly to penalize non-commutativity between $\theta_{0,\ell}$ and $\Delta\theta_\ell$. Empirically, the conflict c_ℓ tends to be higher in shallow layers and significantly decreases with depth across almost all base mergers, as one can observe in the second column in Fig. 2.

3.2.2. Composite weight-only score and gate

We synthesize information (large e_ℓ), conflict (large c_ℓ), and a simple depth prior (r_ℓ) into a single weight-only score defined in Eq. (8):

$$w_\ell = \frac{e_\ell^\eta r_\ell^\rho}{(\text{sp}(z(c_\ell)) + 1)}, z(x_\ell) = \frac{x_\ell - \mu_x}{\sigma_x}, \text{sp}(t) = \log(1 + e^t), \quad (8)$$

where $z(\cdot)$ standardizes a scalar across layers with mean μ_x and standard deviation σ_x , and $\text{sp}(\cdot)$ is softplus. A multiplicative “product-of-experts” form lets e_ℓ and c_ℓ act jointly while r_ℓ encodes the empirical depth trend. We standardize c_ℓ across layers via $z(\cdot)$ so its scale is comparable model-to-model, pass it through softplus to keep the penalty positive and smooth, and add +1 to avoid vanishing denominators while making the mapping monotone in c_ℓ . $\eta, \rho, \zeta \geq 0$ tune the relative influence of each factor. In the paper we choose $\eta=1, \rho=0.5$.

After obtaining w_ℓ , we map it to the per-layer scale using either a robust *tiered* rule (default) or a continuous mapping.

Continuous gate. We convert w_ℓ using a bounded gate function r :

$$s_\ell = r(w_\ell) = 1 + 0.5 \tanh(\gamma(w_\ell - 1)).$$

The tanh nonlinearity yields a smooth, saturating mapping centered at 1 so small w_ℓ perturbations do not cause large changes, while bounding s_ℓ in $(0.5, 1.5)$ prevents pathological over/under-scaling. Across all experiment we set $\gamma=3$. See the third column in Fig. 2 where s_ℓ gradually increases with depth on ViT backbones that account for both information richness and conflict level. The additive constant in the denominator ensures identity scaling for a neutral layer, improves numerical stability, and performance is empirically insensitive to small variations of this offset.

Why bounded scaling and metric design. We constrain $s_\ell \in (0.5, 1.5)$ to avoid pathological scaling in the data-free regime. Under local smoothness along the merge direction, excess loss grows approximately quadratically with scaling deviation, making coarse bounded scaling robust to estimation noise. Effective-rank contrast e_ℓ favors concentrated, low-dimensional updates often associated with informative adaptation, while diffuse high-rank deltas resemble noise and are thus down-weighted. The commutator term c_ℓ measures operator non-commutativity; large values indicate feature-rotating updates that are more prone to interference and therefore benefit from shrinkage.

Tiered gate. Alternatively, we can map these raw weights to discrete layer scaling coefficients s_ℓ via a simple three-level schema. Rather than directly using r_ℓ , which might vary continuously, we assign each layer into one of three categories: shallow, middle, or deep (top) layers, and we use a fixed scale value for each category. In our design, shallow layers receive a down-scaling (e.g. $s_\ell = 0.5$), middle layers use a neutral scaling ($s_\ell = 1.0$), and top layers receive an amplified scaling ($s_\ell = 1.5$). Formally the schema can be defined as follows:

$$s_\ell^{\text{tier}} \in \{0.5, 1.0, 1.5\}, s_\ell^{\text{tier}} = \begin{cases} 0.5, & w_\ell \leq t_1, \\ 1.0, & t_1 < w_\ell \leq t_2, \\ 1.5, & w_\ell > t_2, \end{cases} \quad (9)$$

with fixed thresholds (t_1, t_2) reused across models and mergers. This three-bucket assignment is determined by a non-linear mapping of the raw score and the layer index: for instance, lower-indexed layers tend to fall into the “shallow” bucket unless their r_ℓ is exceptionally high, whereas higher-indexed layers are biased toward the “deep” bucket. The exact boundaries for these buckets are fixed in advance as a part of our recipe (and kept constant for all models and tasks).

To determine (t_1, t_2) , we define the empirical CDF $\hat{F}_L(t) = \frac{1}{|\mathcal{A}|} \sum_{\ell \in \mathcal{A}} \mathbf{1}\{w_\ell \leq t\}$ and set the tier thresholds as the (α, β) quantiles:

$$(t_1, t_2) = \left(\inf\{t : \hat{F}_L(t) \geq \alpha\}, \inf\{t : \hat{F}_L(t) \geq \beta\} \right).$$

Quantiles are scale-free and yield a stable fraction of layers in each bucket irrespective of the absolute range of w_ℓ . Across tasks we choose to use $(\alpha, \beta) = (\frac{1}{3}, \frac{2}{3})$ that gives roughly balanced terciles (shrink / neutral / amplify) and works well across backbones and mergers.

In essence, the combination of the metrics and tanh shaping yields an initial continuous estimate for how aggressively to apply the update at each layer, and then this step collapses that estimate to one of three discrete scaling levels (0.5, 1.0, or 1.5). This discretization adds a smoothing effect that

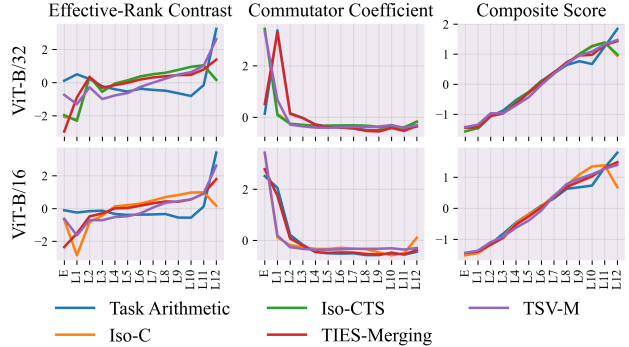


Figure 2. Layer-wise behavior of weight-only metrics. We show effective-rank contrast (e_ℓ), commutator coefficient (c_ℓ), and composite score (s_ℓ) for five data-free merging methods on ViT-B/32 (top) and ViT-B/16 (bottom). Deeper layers exhibit higher e_ℓ and lower c_ℓ , producing monotonically increasing composite scores and motivating our depth-aware scaling rule.

avoids overfitting to idiosyncrasies of a particular model: it forces similar treatment for broad groups of layers (early vs. mid vs. late), which we found generalizes well across architectures.

Depth prior versus weight-only diagnostics. Depth provides a useful coarse prior, but it cannot capture layer-specific structure and conflict. Linear or tiered depth schedules already improve over uniform scaling, yet they apply the same rule to all layers at a given depth. In contrast, the weight-only signals e_ℓ and c_ℓ introduce layer-adaptive modulation based on update structure and operator conflict, respectively. As shown in the ablation study, incorporating these diagnostics consistently outperforms depth-only scaling.

For completeness, we evaluate both the continuous composite-score scaling and the tiered scheme for every merge rule and backbone, and report the stronger of the two variants; a detailed discussion of the tiered search is provided in the appendix. We emphasize that r_ℓ serves only as a simple depth prior with a modest exponent, and is not intended to dominate the composite score; ablations in Sec. 4.4 show that the weight-only diagnostics e_ℓ and c_ℓ each provide additional gains beyond using r_ℓ alone.

3.2.3. Discussion

Putting these components together, Algorithm 1 summarizes our proposed veneer, which can be attached as a training-free add-on to any base merger \mathcal{M} . The layer-wise gating is merger-agnostic and data-free, so the same fixed layer-scaling policy is used across all experiments. Empirically, LARV’s layer-wise adaptation consistently preserves accuracy better than uniform merging, indicating robustness and

Input: Pretrained θ_0 ; task deltas $\{\Delta\theta_{i,\ell}\}$; base merger \mathcal{M} ; exponents (η, ρ, ζ) ; depth prior p ; gate sharpness γ ; *mode* $\in \{\text{tiered, continuous}\}$; tiered quantiles (α, β) ; small $\varepsilon > 0$.

Output: Merged model θ_{LARV} .

for $\ell = 1$ **to** L **do**

1. Merge per-layer deltas.

$$\Delta\theta_\ell \leftarrow \mathcal{M}(\{\Delta\theta_{i,\ell}\}_{i=1}^K) \quad // \text{ Eq. (2)}$$

2. Compute weight-only diagnostics.

Calculate e_ℓ and c_ℓ via Eqs. (5-7)

3. Composite weight-only scores.

Standardize to obtain $z(c_\ell)$ then

$$w_\ell \leftarrow \frac{e_\ell^\eta r_\ell^\rho}{(\text{sp}(z(c_\ell)) + 1)^\zeta} \quad // \text{ Eq. (8)}$$

4A. Tiered gate.

if *mode* *is* *tiered* **then**

 | assign $s_\ell \in \{0.5, 1.0, 1.5\}$ by Eq. (9)

end

4B. Continuous gate.

if *mode* *is* *continuous* **then**

 | $\hat{s}_\ell \leftarrow 1 + 0.5 \tanh(\gamma(w_\ell - 1))$

end

5. Compose the merged model.

$$\theta_{\text{LARV}, \ell} \leftarrow \theta_{0,\ell} + s_\ell \Delta\theta_\ell$$

end

return θ_{LARV} .

Algorithm 1: LARV: data-free layer-wise adaptive rescaling veneer over a base merger

broad applicability.

Conceptually, our method offers a unified view that recovers uniform merging as a special case ($s_1 = \dots = s_L$) while also admitting optional unlabeled probes without any additional learning. It further refines the understanding of model merging by probing the layer-wise structure through two complementary lenses: e_ℓ rewards concentrated updates that stay aligned with base semantics (akin to successful low-rank adaptation [33]), and c_ℓ penalizes order-sensitive interference, a notion complementary to permutation-based alignment [7, 8] and orthogonal to Fisher reweighting and sign-trimming rules [5, 11].

3.3. Complexity and Implementation

LARV introduces computational overhead mainly affected by lightweight randomized SVD. $O(m_\ell n_\ell k L)$ operations where m_ℓ and n_ℓ are the dimensions of each layer’s matrices and k is the rank of the matrices, for computing (e_ℓ, c_ℓ) and applying per-layer scaling. No additional gradients or

memory copies are required. The implementation can be completed in under 20 lines of Python and integrates seamlessly into the FusionBench [20] framework.

No merge-time tuning. Although LARV introduces coefficients $(\eta, \rho, \zeta, \gamma)$, these are not merge-time tuning knobs. All experiments use one fixed configuration across tasks, backbones, and base mergers, with no gradients, validation sets, or task-specific search. Sensitivity analysis (Appendix) shows performance remains stable across wide parameter ranges, indicating that LARV operates in a robust, no-tuning regime.

4. Results and Analysis

4.1. Experimental Setup

We evaluate **LARV merging** on CLIP ViT [39] backbones **B/32**, **B/16**, and **L/14** under three merge settings [26, 30] with **8 Tasks**, **14 Tasks**, and **20 Tasks** classification tasks using FusionBench [20]. For the 8-task suite we report per-dataset scores on **SUN397** [40], **Stanford Cars** [41], **RESISC45** [42], **EuroSAT** [43], **SVHN** [44], **GTSRB** [45], **MNIST** [46], and **DTD** [47]. We compare to representative training-free baselines: *Simple Averaging*, *Task Arithmetic (TA)*, *ISO-C* and *ISO-CTS* [48], *TIES-Merging* [11], and *TSV-M* [27]. LARV is used as a *veneer* on each base rule (e.g., “TIES/LARV”): the only change is replacing the uniform scale in Eq. (2) with the layer-wise scales in Eq. (3). No data and no retraining are used anywhere. All numbers are top-1 accuracy (%) with the average taken over tasks in each block. Parentheses in LARV rows denote the absolute gain over the corresponding base rule.

4.2. Main Results Across Backbones (8 tasks)

Table 1 presents the full 8-task results for ViT-B/32, ViT-B/16, and ViT-L/14. Across all three backbones and all merge rules, applying the LARV veneer leads to a consistent improvement over the underlying baseline. The magnitude of the gain varies with the strength of the base rule, but the trend is uniform: weaker methods such as TA and TIES benefit the most, while stronger baselines such as Iso-C, Iso-CTS, and TSV-M obtain smaller yet reliable boosts.

A clear pattern appears across backbones. LARV produces its largest improvements on datasets where layer-wise heterogeneity is more pronounced, such as *RESISC45*, *EuroSAT*, and *GTSRB*. These tasks rely more heavily on deeper visual representations, and the depth-dependent scaling provided by LARV helps stabilize the merge and reduce cross-layer conflict. Meanwhile, high-accuracy datasets such as *MNIST* and *SVHN* remain near ceiling, indicating that the veneer does not disturb layers that already align well.

Method	SUN397	Cars	RESISC45	EuroSAT	SVHN	GTSRB	MNIST	DTD	Avg.
ViT-B/32									
<i>fine-tuned</i>	74.9	78.5	95.1	99.1	97.3	98.9	99.6	79.7	90.4
AdaMerging	59.2	57.9	70.6	79.3	70.5	54.3	—	—	68.1
Simple Averaging	65.4	62.4	70.6	75.7	64.5	55.0	86.3	50.6	66.3
TA/LARV	60.1 (+3.1)	64.9 (+9.2)	73.3 (+8.5)	87.9 (+14.6)	81.1 (+3.2)	76.9 (+8.4)	97.3 (+1.2)	55.9 (+8.7)	74.7 (+7.1)
ISO-C/LARV	70.9 (+1.2)	75.6 (+2.7)	90.0 (+4.0)	96.1 (+6.4)	86.5 (-1.1)	94.6 (+2.2)	98.8 (+0.3)	74.4 (+9.0)	85.9 (+3.1)
ISO-CTS/LARV	72.9 (+1.8)	76.4 (+1.8)	90.3 (+3.8)	93.4 (+4.3)	81.6 (-1.8)	91.4 (+1.0)	98.3 (+0.2)	74.5 (+0.6)	84.9 (+2.1)
TIES/LARV	68.7 (+1.7)	67.9 (+3.7)	79.6 (+5.3)	84.9 (+10.4)	77.8 (+0.0)	76.3 (+6.9)	95.4 (+1.3)	58.9 (+4.9)	76.2 (+4.3)
TSV-M/LARV	69.9 (+2.3)	74.9 (+3.2)	88.5 (+3.8)	95.6 (+2.2)	90.1 (-1.8)	92.7 (+0.2)	98.9 (+0.0)	70.9 (+7.0)	85.2 (+2.1)
ViT-B/16									
<i>fine-tuned</i>	78.9	85.9	96.6	99.1	97.6	99.0	99.7	82.3	92.3
AdaMerging	67.1	65.7	78.7	86.0	86.8	91.6	96.4	45.2	45.2
Simple Averaging	68.7	69.0	75.1	83.3	75.0	62.6	93.8	51.2	72.3
TA/LARV	66.1 (+0.2)	71.6 (+3.3)	78.1 (+2.6)	86.7 (+2.2)	89.4 (+0.6)	84.3 (+2.3)	98.6 (+0.5)	58.1 (+4.1)	79.1 (+2.0)
ISO-C/LARV	76.7 (+0.9)	85.3 (+2.5)	93.2 (+0.9)	96.9 (+0.6)	91.0 (-0.8)	94.9 (-0.1)	98.8 (-0.1)	76.8 (+4.8)	89.2 (+1.1)
ISO-CTS/LARV	75.5 (-0.6)	83.2 (-0.6)	93.4 (+0.8)	97.2 (+1.2)	93.4 (+2.5)	96.6 (+1.9)	98.9 (+0.3)	74.7 (+1.0)	89.1 (+0.8)
TIES/LARV	72.2 (+1.5)	73.2 (+2.0)	84.8 (+4.9)	90.6 (+3.1)	90.9 (+7.6)	87.6 (+11.3)	98.3 (+1.9)	61.1 (+5.6)	82.3 (+4.7)
TSV-M/LARV	74.0 (+0.9)	82.6 (+1.9)	91.3 (+1.6)	96.6 (+0.4)	93.1 (-1.0)	93.7 (-0.4)	99.1 (+0.0)	75.4 (+5.7)	88.2 (+1.1)
ViT-L/14									
<i>fine-tuned</i>	82.8	92.8	97.4	99.1	97.9	99.2	99.8	85.5	94.3
AdaMerging	75.9	80.2	78.1	82.0	68.3	93.2	93.1	68.6	79.9
Simple Averaging	72.5	81.5	82.3	88.5	81.6	74.0	96.6	61.8	79.9
TA/LARV	74.5 (+2.5)	83.3 (+4.3)	86.2 (+5.6)	92.7 (+8.1)	88.9 (+1.4)	88.8 (+5.3)	98.6 (+0.6)	63.8 (+5.3)	84.6 (+4.1)
ISO-C/LARV	80.8 (+0.1)	92.4 (+0.9)	95.9 (+0.5)	97.5 (+0.3)	94.6 (-0.6)	97.8 (+0.0)	99.2 (+0.1)	82.9 (+2.6)	92.6 (+0.5)
ISO-CTS/LARV	81.4 (+0.3)	93.0 (+0.8)	96.4 (+0.8)	97.6 (+0.3)	94.1 (-0.5)	97.3 (-0.2)	99.2 (+0.1)	83.6 (+2.5)	92.8 (+0.5)
TIES/LARV	77.3 (+2.6)	86.7 (+3.5)	91.1 (+4.6)	94.4 (+4.7)	88.9 (-0.8)	88.8 (+3.6)	98.2 (+0.4)	68.7 (+4.8)	86.7 (+2.9)
TSV-M/LARV	79.8 (+1.6)	91.0 (+1.2)	94.4 (+0.9)	97.8 (+1.1)	95.2 (-0.4)	96.9 (+0.4)	99.2 (+0.1)	79.5 (+4.2)	91.7 (+1.1)

Table 1. ViT results on 8 classification tasks for ViT-B/32, ViT-B/16, and ViT-L/14. All numbers are percentages. For each LARV variant, the gray parenthetical value shows its performance gain relative to the corresponding baseline, allowing the baseline score to be implicitly recovered. Blue indicates a positive gain, while red denotes a decrease in accuracy.

Method	ViT-B/32			ViT-B/16			ViT-L/14		
	8 Tasks	14 Tasks	20 Tasks	8 Tasks	14 Tasks	20 Tasks	8 Tasks	14 Tasks	20 Tasks
Pretrained	48.3	57.2	56.1	55.3	61.3	59.7	64.7	68.2	65.2
Fine-tuned	92.8	90.9	91.3	94.6	92.8	93.2	95.8	94.3	94.7
TA/LARV	73.8 (+6.3)	65.8 (+13.0)	83.3 (+19.2)	79.1 (+2.0)	73.3 (+12.5)	88.6 (+23.7)	84.6 (+4.1)	76.3 (+13.2)	55.0 (+19.0)
ISO-C/LARV	85.9 (+3.1)	81.2 (+3.1)	93.9 (+2.6)	89.2 (+1.1)	84.3 (+1.9)	96.1 (+1.2)	92.6 (+0.5)	90.5 (+1.0)	85.4 (+2.0)
ISO-CTS/LARV	84.9 (+2.2)	82.4 (+3.0)	94.6 (+2.2)	89.1 (+0.8)	86.1 (+1.6)	96.1 (+0.9)	92.8 (+0.5)	91.1 (+0.7)	87.3 (+1.5)
TIES/LARV	76.3 (+4.4)	73.6 (+6.0)	91.5 (+5.2)	82.3 (+4.7)	77.3 (+5.8)	94.7 (+4.7)	86.7 (+2.9)	83.7 (+5.9)	70.4 (+7.4)
TSV-M/LARV	83.1 (+6.6)	81.2 (+2.4)	94.6 (+1.3)	88.2 (+1.1)	84.2 (+2.1)	96.2 (+1.1)	91.7 (+1.1)	89.8 (+1.6)	86.4 (+3.2)

Table 2. **Performance summary on 8/14/20 tasks.** Average accuracy (%) for each ViT backbone across 8/14/20-task merges. Blue numbers denote the absolute improvement of each LARV variant over the corresponding baseline without LARV. The results show that LARV consistently boosts all merging rules, with larger gains appearing on smaller backbones (ViT-B/32, ViT-B/16) and more challenging merge settings (20 tasks).

r_ℓ	e_ℓ	c_ℓ	TIES	Iso-C	Iso-CTS	TSV-M
—	—	—	0.719	0.828	0.827	0.831
—	—	✓	0.734	0.833	0.833	0.830
✓	—	—	0.751	0.847	0.851	0.846
✓	—	✓	0.756	0.848	0.851	0.846
✓	✓	✓	0.759	0.850	0.854	0.850

Table 3. Ablation on layer metrics r_ℓ, e_ℓ, c_ℓ and their effect on several merging baselines.

Key Observations. (1) LARV improves every backbone and every merge rule, with gains ranging from small but con-

sistent (Iso-CTS, TSV-M) to substantial (TA, TIES). (2) Improvements concentrate on tasks that depend more strongly on mid-to-deep layers, consistent with the intended effect of LARV’s depth-aware scaling. (3) Performance is stable across model layers (B/32, B/16, L/14), suggesting that the three-signal layer scaling generalizes reliably as backbone capacity grows.

4.3. Summary Across Backbones and Task Scales

Table 2 summarizes average accuracies for the three ViT backbones under 8-, 14-, and 20-task merges. Each cell reports the merged accuracy and the absolute gain achieved

by attaching the LARV veneer to the corresponding baseline. Across all settings, LARV consistently improves every base rule, including Task Arithmetic, ISO-C/CTS, TIES-Merging, and TSV-M.

Scale across model size. Gains are largest on smaller backbones (e.g., ViT-B/32), which are more sensitive to cross-task interference and therefore benefit more from suppressing shallow-layer noise and amplifying deeper-layer structure.

Scale with merge difficulty. LARV brings noticeably larger gains in more challenging scenarios, especially in the 20-task experiments where interference between models is strongest and uniform scaling often falls short. This pattern indicates that layer-wise adaptation becomes increasingly important as the number of merged tasks grows.

Taken together, the results show that LARV scales well with both model capacity (from B/32 to L/14) and merge difficulty (from 8 to 20 tasks), delivering consistent improvements across architectures without requiring data or extra tuning.

4.4. Ablation on Weight-Only Metrics (r_ℓ, e_ℓ, c_ℓ)

We ablate the three weight-only components used in LARV’s composite score: the depth prior r_ℓ , the information signal e_ℓ , and the conflict signal c_ℓ . Table 3 evaluates all valid combinations of these terms across four representative baselines: TIES-Merging, ISO-C, ISO-CTS, and TSV-M.

Across all methods, the trend is consistent. Using none of the signals yields the weakest performance, confirming that layer-wise variability is essential for effective merging. Adding the depth prior r_ℓ alone already recovers a substantial portion of the overall gain, reflecting the broad depth-related structure in ViT updates. Introducing e_ℓ further improves accuracy by elevating layers whose updates contain more structured, informative variation. The conflict term c_ℓ provides an additional refinement by suppressing non-commutative, interference-prone updates.

When all three terms (r_ℓ, e_ℓ, c_ℓ) are used together, each baseline achieves its strongest or near-strongest result. This demonstrates that LARV is not simply a hand-crafted depth schedule: r_ℓ explains part of the improvement, but both e_ℓ and c_ℓ contribute complementary information that cannot be recovered from depth alone. Overall, the full combination yields the most stable and effective layer-wise scaling.

4.5. Robustness under Input Corruptions

We further evaluate robustness using a set of common input corruptions (blurring, noise, and digital artifacts), following the ImageNet-C convention[17]. For each corruption type we measure accuracy across severities and report the mean in Fig. 3. Across all four merge rules, applying LARV yields a consistent improvement over the corresponding baseline. The gains are most visible on corruptions that strongly affect

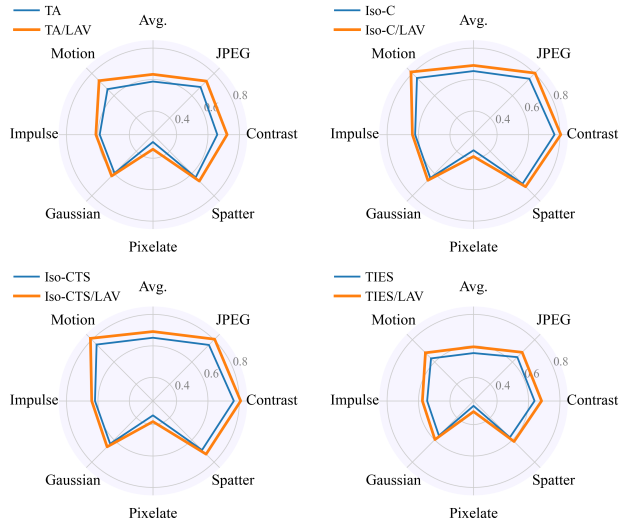


Figure 3. Performance on 7 corruption types and overall average. LARV consistently improves robustness across all corruption methods.

low-level structure, such as Motion, Impulse, and Gaussian noise, where suppressing shallow-layer responses reduces the propagation of spurious activations. Improvements are also observed on more feature-oriented corruptions such as Contrast and JPEG, indicating that the depth-dependent scaling helps preserve mid- and high-level representations even when the input distribution is perturbed.

The effect is uniform across rules: TA, Iso-C, Iso-CTS, and TIES each benefit from LARV, and no degradation is observed on any corruption type. This stability is noteworthy because the veneer is applied without retraining or corruption-aware tuning. Combined with the clean-data results, these findings demonstrate that the proposed layer-wise scaling not only mitigates cross-layer interference but also enhances resilience under distribution shift.

4.6. Generalization to Unseen Tasks

We further assess whether the benefits of LARV extend beyond the task suite used to construct the task-vectors. Table 4 reports results for ViT-B/32 on eight seen tasks and two additional unseen evaluation datasets. The comparison includes Fisher Merging, RegMean, RegMean++, and layer-wise AdaMerging.

Across all baselines, adding the LARV veneer consistently improves performance on the seen tasks, with notable gains on RESISC45, DTD, and GTSRB. These improvements also transfer to the unseen datasets: LARV-enhanced variants obtain higher accuracy on MNIST and EuroSAT without any retraining or domain-specific adjustments. The consistency of these gains indicates that LARV reduces cross-layer interference in a manner that generalizes across datasets, rather than relying on characteristics specific to the

Method	Seen Tasks							Unseen Tasks		
	SUN397	Cars	RESISC45	DTD	SVHN	GTSRB	Avg.	MNIST	EuroSAT	Avg.
<i>Pre-trained</i>	63.2	59.9	60.6	43.9	ViT-B/32 Generalization			47.6	45.6	46.6
					23.5	30.4	46.9			
Fisher Merging	65.5	67.2	78.2	57.6	84.2	75.9	71.4	71.8	49.4	60.6
RegMean	69.5	70.8	88.7	67.2	95.2	89.4	80.1	82.9	44.6	63.8
RegMean++	69.8	70.8	90.2	70.3	95.5	93.2	81.6	81.3	44.1	62.7
Layer-wise AdaMerging	68.4	71.9	87.9	69.1	92.2	93.8	80.5	77.7	47.3	62.5
TSV-M/LARV	70.1 (+1.0)	75.5 (+2.7)	91.6 (+3.3)	71.2 (+4.6)	94.1 (-0.4)	95.1 (-0.2)	82.9 (+1.8)	86.2 (+1.8)	49.6 (+3.0)	67.9 (+2.2)
TA/LARV	65.9 (+1.7)	67.2 (+4.2)	79.7 (+6.5)	59.6 (+4.9)	86.2 (+1.5)	84.0 (+4.5)	73.8 (+3.9)	78.4 (+3.0)	43.2 (+2.5)	60.8 (+2.7)
ISO-C/LARV	74.4 (+2.3)	78.3 (+3.9)	92.2 (+4.2)	73.5 (+5.4)	85.2 (-0.5)	93.2 (+1.4)	82.8 (+2.8)	80.9 (+2.3)	56.4 (+3.3)	68.6 (+2.7)
ISO-CTS/LARV	74.2 (+2.5)	78.4 (+4.1)	92.5 (+4.7)	75.0 (+5.1)	83.8 (+0.3)	93.5 (+1.7)	82.9 (+3.1)	79.0 (+1.9)	57.4 (+5.0)	68.2 (+3.4)
TIES/LARV	69.9 (+1.8)	67.8 (+2.1)	81.6 (+5.1)	59.1 (+4.2)	76.3 (+0.9)	77.8 (+5.7)	72.1 (+3.3)	74.1 (+1.1)	49.5 (+2.6)	61.8 (+1.8)

Table 4. Generalization results for ViT-B/32 on both seen and unseen tasks. All numbers are percentages. Parenthetical values indicate performance gain relative to the corresponding baseline without LARV. LARV consistently improves in-distribution accuracy while also enhancing cross-task generalization to unseen datasets (MNIST, EuroSAT) without any retraining.

tasks used during merge construction.

5. Conclusion

We introduced LARV, a data-free, training-free layer-wise rescaling veneer that improves model merging by replacing a single global coefficient with depth-aware scales derived from two simple weight-only diagnostics, information richness e_ℓ and conflict level c_ℓ . Across all ViT backbones and merge sizes, LARV consistently enhances Task Arithmetic, ISO-C/CTS, TIES-Merging, and TSV-M, with the largest gains appearing on smaller models and harder 20-task merges. It further improves robustness under input corruptions and generalizes to unseen tasks without any tuning. These results show that acknowledging depth heterogeneity is an effective inductive bias for training-free merging, turning task-vector composition into a more stable and structurally informed procedure.

References

- [1] R. Bommasani, “On the opportunities and risks of foundation models,” *arXiv preprint arXiv:2108.07258*, 2021. 1
- [2] M. Yurochkin, M. Agarwal, S. Ghosh, K. Greenewald, N. Hoang, and Y. Khazaeni, “Bayesian nonparametric federated learning of neural networks,” in *International conference on machine learning*, pp. 7252–7261, PMLR, 2019. 1
- [3] Z. Zheng, M. Ma, K. Wang, Z. Qin, X. Yue, and Y. You, “Preventing zero-shot transfer degradation in continual learning of vision-language models,” in *Proceedings of the IEEE/CVF international conference on computer vision*, pp. 19125–19136, 2023. 1
- [4] M. Wortsman, G. Ilharco, S. Y. Gadre, R. Roelofs, R. Gontijo-Lopes, A. S. Morcos, H. Namkoong, A. Farhadi, Y. Carmon, S. Kornblith, *et al.*, “Model soups: averaging weights of multiple fine-tuned models improves accuracy without increasing inference time,” in *International conference on machine learning*, pp. 23965–23998, PMLR, 2022. 1, 2, 3
- [5] M. S. Matena and C. A. Raffel, “Merging models with fisher-weighted averaging,” *Advances in Neural Information Processing Systems*, vol. 35, pp. 17703–17716, 2022. 1, 2, 3, 6
- [6] G. Ilharco, M. T. Ribeiro, M. Wortsman, S. Gururangan, L. Schmidt, H. Hajishirzi, and A. Farhadi, “Editing models with task arithmetic,” *arXiv preprint arXiv:2212.04089*, 2022. 2
- [7] S. K. Ainsworth, J. Hayase, and S. S. Srinivasa, “Git rebasin: Merging models modulo permutation symmetries,” in *International Conference on Learning Representations*, 2023. 1, 2, 3, 6
- [8] R. Entezari, H. Sedghi, O. Saukh, and B. Neyshabur, “The role of permutation invariance in linear mode connectivity of neural networks,” *arXiv preprint arXiv:2110.06296*, 2021. 1, 2, 3, 6
- [9] B. McMahan, E. Moore, D. Ramage, S. Hampson, and B. A. y Arcas, “Communication-efficient learning of deep networks from decentralized data,” in *Proceedings of the 20th International Conference on Artificial Intelligence and Statistics*, vol. 54 of *Proceedings of Machine Learning Research*, pp. 1273–1282, PMLR, 2017. 1
- [10] E. Yang, L. Shen, G. Guo, X. Wang, X. Cao, J. Zhang, and D. Tao, “Model merging in llms, mllms, and beyond: Methods, theories, applications and opportunities,” *arXiv preprint arXiv:2408.07666*, 2024. 1
- [11] P. Yadav, D. Tam, L. Choshen, C. A. Raffel, and M. Bansal, “Ties-merging: Resolving interference when merging models,” *Advances in Neural Information Processing Systems*, vol. 36, pp. 7093–7115, 2023. 1, 3, 6
- [12] G. Du, J. Lee, J. Li, R. Jiang, Y. Guo, S. Yu, H. Liu, S. K. Goh, H.-K. Tang, D. He, and M. Zhang, “Parameter competition balancing for model merging,” *Advances in Neural Information Processing Systems*, vol. 37, pp. 84746–84776, 2024. 1
- [13] J. Yosinski, J. Clune, Y. Bengio, and H. Lipson, “How transferable are features in deep neural networks?,” in *Advances in Neural Information Processing Systems*, vol. 27, 2014. 1, 2, 3
- [14] M. D. Zeiler and R. Fergus, “Visualizing and understanding convolutional networks,” in *European Conference on Com-*

- puter Vision, vol. 8689 of *Lecture Notes in Computer Science*, pp. 818–833, Springer, 2014. 2
- [15] S. Kornblith, M. Norouzi, H. Lee, and G. Hinton, “Similarity of neural network representations revisited,” in *Proceedings of the 36th International Conference on Machine Learning*, vol. 97 of *Proceedings of Machine Learning Research*, pp. 3519–3529, PMLR, 2019. 4
- [16] M. Raghu, J. Gilmer, J. Yosinski, and J. Sohl-Dickstein, “Svcca: Singular vector canonical correlation analysis for deep learning dynamics and interpretability,” *Advances in neural information processing systems*, vol. 30, 2017. 1, 3, 4
- [17] D. Hendrycks and T. Dietterich, “Benchmarking neural network robustness to common corruptions and perturbations,” *arXiv preprint arXiv:1903.12261*, 2019. 1, 3, 8
- [18] R. Geirhos, J.-H. Jacobsen, C. Michaelis, R. Zemel, W. Brendel, M. Bethge, and F. A. Wichmann, “Shortcut learning in deep neural networks,” *Nature Machine Intelligence*, vol. 2, no. 11, pp. 665–673, 2020. 1, 3
- [19] Y. Idelbayev and M. A. Carreira-Perpinán, “Low-rank compression of neural nets: Learning the rank of each layer,” in *Proceedings of the IEEE/CVF conference on computer vision and pattern recognition*, pp. 8049–8059, 2020. 1
- [20] A. Tang, L. Shen, Y. Luo, H. Hu, B. Du, and D. Tao, “Fusion-bench: A comprehensive benchmark of deep model fusion,” *arXiv preprint arXiv:2406.03280*, 2024. 2, 6
- [21] P. Izmailov, D. Podoprikin, T. Garipov, D. Vetrov, and A. G. Wilson, “Averaging weights leads to wider optima and better generalization,” *arXiv preprint arXiv:1803.05407*, 2018. 2
- [22] X. Jin, X. Ren, D. Preotiu-Pietro, and P. Cheng, “Dataless knowledge fusion by merging weights of language models,” *arXiv preprint arXiv:2212.09849*, 2022. 2, 3
- [23] W. Sun, Q. Li, Y.-a. Geng, and B. Li, “Cat merging: A training-free approach for resolving conflicts in model merging,” *arXiv preprint arXiv:2505.06977*, 2025. 3
- [24] F. Xiong, R. Cheng, W. Chen, Z. Zhang, Y. Guo, C. Yuan, and R. Xu, “Multi-task model merging via adaptive weight disentanglement,” *arXiv preprint arXiv:2411.18729*, 2024. 3
- [25] L. Yu, B. Yu, H. Yu, F. Huang, and Y. Li, “Language models are super mario: Absorbing abilities from homologous models as a free lunch,” in *Forty-first International Conference on Machine Learning*, 2024. 3
- [26] C. Huang, P. Ye, T. Chen, T. He, X. Yue, and W. Ouyang, “Emr-merging: Tuning-free high-performance model merging,” *Advances in Neural Information Processing Systems*, vol. 37, pp. 122741–122769, 2024. 3, 6
- [27] A. A. Gargiulo, D. Crisostomi, M. S. Bucarelli, S. Scardapane, F. Silvestri, and E. Rodola, “Task singular vectors: Reducing task interference in model merging,” in *Proceedings of the Computer Vision and Pattern Recognition Conference*, pp. 18695–18705, 2025. 3, 6
- [28] P. Ye, C. Huang, M. Shen, T. Chen, Y. Huang, Y. Zhang, and W. Ouyang, “Merging vision transformers from different tasks and domains,” *arXiv preprint arXiv:2312.16240*, 2023. 3
- [29] E. Yang, Z. Wang, L. Shen, S. Liu, G. Guo, X. Wang, and D. Tao, “Adamerging: Adaptive model merging for multi-task learning,” *arXiv preprint arXiv:2310.02575*, 2023. 3
- [30] Z. Lu, C. Fan, W. Wei, X. Qu, D. Chen, and Y. Cheng, “Twin-merging: Dynamic integration of modular expertise in model merging,” *Advances in Neural Information Processing Systems*, vol. 37, pp. 78905–78935, 2024. 3, 6
- [31] S. Chen, C. Ge, Z. Tong, J. Wang, Y. Song, J. Wang, and P. Luo, “Adaptformer: Adapting vision transformers for scalable visual recognition,” *Advances in Neural Information Processing Systems*, vol. 35, pp. 16664–16678, 2022. 3
- [32] N. Houlsby, A. Giurgiu, S. Jastrzebski, B. Morrone, Q. De Laroussilhe, A. Gesmundo, M. Attariyan, and S. Gelly, “Parameter-efficient transfer learning for nlp,” in *International conference on machine learning*, pp. 2790–2799, PMLR, 2019.
- [33] E. J. Hu, Y. Shen, P. Wallis, Z. Allen-Zhu, Y. Li, S. Wang, L. Wang, W. Chen, *et al.*, “Lora: Low-rank adaptation of large language models,” *International Conference on Learning Representations*, vol. 1, no. 2, p. 3, 2022. 6
- [34] E. B. Zaken, Y. Goldberg, and S. Ravfogel, “Bitfit: Simple parameter-efficient fine-tuning for transformer-based masked language-models,” in *Proceedings of the 60th Annual Meeting of the Association for Computational Linguistics (Volume 2: Short Papers)*, pp. 1–9, 2022.
- [35] Z. Zhao, T. Shen, D. Zhu, Z. Li, J. Su, X. Wang, K. Kuang, and F. Wu, “Merging loras like playing lego: Pushing the modularity of lora to extremes through rank-wise clustering,” *arXiv preprint arXiv:2409.16167*, 2024. 3
- [36] B. Qi, F. Li, Z. Wang, J. Gao, D. Li, P. Ye, and B. Zhou, “Less is more: Efficient model merging with binary task switch,” in *Proceedings of the Computer Vision and Pattern Recognition Conference*, pp. 15265–15274, 2025. 3
- [37] T.-H. Nguyen, D. Huu-Tien, T. Suzuki, and L.-M. Nguyen, “Regmean++: Enhancing effectiveness and generalization of regression mean for model merging,” *arXiv preprint arXiv:2508.03121*, 2025. 3
- [38] H. Wang, C. Ma, I. Almakky, I. Reid, G. Carneiro, and M. Yaqub, “Rethinking weight-averaged model-merging,” *arXiv preprint arXiv:2411.09263*, 2024. 3
- [39] A. Radford, J. W. Kim, C. Hallacy, A. Ramesh, G. Goh, S. Agarwal, G. Sastry, A. Askell, P. Mishkin, J. Clark, *et al.*, “Learning transferable visual models from natural language supervision,” in *International conference on machine learning*, pp. 8748–8763, PmLR, 2021. 6
- [40] J. Xiao, J. Hays, K. A. Ehinger, A. Oliva, and A. Torralba, “Sun database: Large-scale scene recognition from abbey to zoo,” in *2010 IEEE computer society conference on computer vision and pattern recognition*, pp. 3485–3492, IEEE, 2010. 6
- [41] J. Krause, M. Stark, J. Deng, and L. Fei-Fei, “3d object representations for fine-grained categorization,” in *Proceedings of the IEEE international conference on computer vision workshops*, pp. 554–561, 2013. 6
- [42] G. Cheng, J. Han, and X. Lu, “Remote sensing image scene classification: Benchmark and state of the art,” *Proceedings of the IEEE*, vol. 105, no. 10, pp. 1865–1883, 2017. 6
- [43] P. Helber, B. Bischke, A. Dengel, and D. Borth, “Eurosat: A novel dataset and deep learning benchmark for land use and land cover classification,” *IEEE Journal of Selected Topics*

in *Applied Earth Observations and Remote Sensing*, vol. 12, no. 7, pp. 2217–2226, 2019. [6](#)

- [44] Y. Netzer, T. Wang, A. Coates, A. Bissacco, B. Wu, A. Y. Ng, *et al.*, “Reading digits in natural images with unsupervised feature learning,” in *NIPS workshop on deep learning and unsupervised feature learning*, vol. 2011, p. 7, Granada, 2011. [6](#)
- [45] J. Stallkamp, M. Schlipsing, J. Salmen, and C. Igel, “The german traffic sign recognition benchmark: a multi-class classification competition,” in *The 2011 international joint conference on neural networks*, pp. 1453–1460, IEEE, 2011. [6](#)
- [46] Y. LeCun, “The mnist database of handwritten digits,” <http://yann.lecun.com/exdb/mnist/>, 1998. [6](#)
- [47] M. Cimpoi, S. Maji, I. Kokkinos, S. Mohamed, and A. Vedaldi, “Describing textures in the wild,” in *Proceedings of the IEEE conference on computer vision and pattern recognition*, pp. 3606–3613, 2014. [6](#)
- [48] D. Marczak, S. Magistri, S. Cygert, B. Twardowski, A. D. Bagdanov, and J. van de Weijer, “No task left behind: Isotropic model merging with common and task-specific subspaces,” *arXiv preprint arXiv:2502.04959*, 2025. [6](#)

Supplementary Material

A. Formal Definitions and Default Hyperparameters

A.1. Definitions of r_ℓ , $r(\cdot)$, and ζ

In section 3.2.2 We refer the depth prior r_ℓ , the gate mapping $r(\cdot)$, and ζ in compositing weight-only score and gate. For completeness and reproducibility, we provide the formal definitions of r_ℓ and ζ used in the continuous variant, and the exponent ζ in the composite score of Eq. (8).

Depth prior r_ℓ . We define r_ℓ as the normalized layer index:

$$r_\ell = \frac{\ell}{L},$$

where $\ell \in \{1, \dots, L\}$ and L is the total number of parameterized layers. Thus r_ℓ increases monotonically from shallow to deep layers and remains independent of any task or model.

The quantity r_ℓ provides a mild monotonic depth prior that reflects the empirical observation that deeper layers tend to exhibit more stable and semantically meaningful updates. It is not intended to dominate the composite score; instead, the weight-only diagnostics e_ℓ and c_ℓ contribute the majority of the layer-wise variation, as confirmed by the ablations in Table 3.

Gate function $r(\cdot)$ in the continuous variant. In the continuous version of LARV, the raw composite score w_ℓ is mapped to a bounded scaling coefficient s_ℓ via the gate function

$$s_\ell = r(w_\ell) = 1 + 0.5 \tanh(\gamma(w_\ell - 1)),$$

where $\gamma > 0$ controls sharpness. Throughout all experiments we set $\gamma = 3$ for the continuous variant. Note that γ is not used in the tiered version, which directly discretizes w_ℓ using the (α, β) quantiles instead of applying the smooth gate.

Exponent ζ . The exponent ζ balances the influence of the conflict-related term $(sp(z(c_\ell)) + 1)$ within the product-of-experts composite score:

$$w_\ell = e_\ell^\eta r_\ell^\rho (sp(z(c_\ell)) + 1)^\zeta.$$

We fix $\zeta = 1$ for all experiments. This keeps the conflict penalty linear in the standardized commutator score and avoids over-emphasizing noisier layers.

Default hyperparameters. Unless otherwise specified, we use the configuration $(\eta, \rho, \zeta) = (1, 0.5, 1)$ across all backbones, task counts, and merge rules. These values were chosen for simplicity and robustness and were not tuned per model.

B. Additional Details on Complexity

We elaborate the details of complexity in section 3.3.

Randomized SVD setup. For each layer ℓ , LARV computes two quantities (e_ℓ, c_ℓ) based on a lightweight randomized SVD of the weight difference matrix $W_\ell \in \mathbb{R}^{m_\ell \times n_\ell}$. Let k denote the target rank and let α denote the oversampling parameter used in the randomized sketch (typically $\alpha \in [5, 20]$). The sketches therefore operate on a subspace of dimension $k' = k + \alpha$.

Computational complexity. The standard complexity of a single randomized SVD is

$$O(m_\ell n_\ell k') + O(n_\ell k'^2),$$

where the first term corresponds to the randomized projection and the second to the QR/SVD of the sketched matrix. Because $k' \ll \min(m_\ell, n_\ell)$ in all practical settings, the first term dominates and yields

$$O(m_\ell n_\ell (k + \alpha)).$$

Simplified expression used in the main paper. Since α is a small constant independent of model size and k is fixed across layers, we simplify the expression in the main paper as

$$O(m_\ell n_\ell k L),$$

where L is the number of layers. This notation captures the correct scaling with respect to matrix size and number of layers while omitting lower-order constants (α) for clarity.

Choice of k and α . In all experiments we set $k \in \{1, 2\}$ depending on the matrix shape, and we use a constant oversampling $\alpha = 10$ following standard recommendations in randomized numerical linear algebra. We do not perform power iterations, so the above complexity is tight. We emphasize that LARV does not require backpropagation, gradient computation, or additional memory copies; the randomized SVD is applied once per layer and the resulting scaling factors are stored as scalars.

C. Experimental Setup and Protocol

C.1. FusionBench Configuration and Evaluation Protocol

All experiments utilize the **FusionBench** platform to evaluate the LARV across three **CLIP Vision Transformers** (ViT-B/32, ViT-B/16, ViT-L/14). Merging is assessed in three multi-task scenarios: the canonical 8-task, the challenging 14-task, and the high-interference 20-task classification suites.

Strategy	TIES			ISO-C			ISO-CTS			TSV-M		
	B/32	B/16	L/14	B/32	B/16	L/14	B/32	B/16	L/14	B/32	B/16	L/14
Uniform (basecube)	71.9	77.6	83.8	82.8	88.1	92.1	82.7	88.3	92.3	83.1	87.1	90.6
Linear	75.9	79.1	85.7	85.2	88.6	92.4	85.5	89.1	92.8	85.0	88.1	91.6
Composite Score	77.4	79.2	86.6	85.7	79.3	87.5	86.0	79.5	87.9	84.8	87.7	91.6
Tier 12	75.8	79.1	85.7	85.1	88.6	92.4	85.5	89.1	92.8	85.0	88.1	91.6
Tier 6	76.0	79.2	85.9	85.3	88.7	92.4	85.7	89.1	92.8	85.1	88.2	91.7
Tier 3	76.3	79.3	86.1	85.4	88.8	92.5	85.6	89.2	92.8	85.1	88.2	91.7
Tier 2	76.2	79.2	86.2	85.5	88.4	92.3	85.8	88.9	92.6	84.8	87.7	91.6

Table 5. Layer-wise scaling strategy comparison across ViT-B/32, ViT-B/16, and ViT-L/14 (8-task accuracy, %). Depth-only heuristics include linear and multi-stage tiered splits (2/3/6/12). Composite uses EER/CCC-derived adaptive scaling and provides consistent improvements.

Primary Metric. Performance is measured by **Top-1 Accuracy** (in %). Results for the multi-task suites are reported as the **arithmetic mean** of the Top-1 accuracies across all K tasks within that setting.

Robustness and Generalization. We evaluate robustness under distribution shift following the ImageNet-C protocol, testing seven common corruption types (Motion, Impulse, Gaussian, Pixelate, Spatter, Contrast, and JPEG) across four datasets. The main paper reports only the average corruption performance for clarity (Sec. 4.5), while the complete per-corruption results and detailed analysis for all datasets are included in Appendix E.1. We additionally assess generalization by evaluating the merged models on two **unseen tasks** not used in constructing the task vectors.

C.2. Hyperparameters and Implementation Details

All baselines are run with the hyperparameter choices suggested in their original implementations, which we take as the default values in our evaluations.

- **Task Arithmetic:** global coefficient 0.3.
- **Iso-C:** the merge strength increases slightly with model size; we use factors of 1.30, 1.40, and 1.50 for ViT-B/32, ViT-B/16, and ViT-L/14, respectively.
- **Iso-CTS:** scaling 1.5 following the recommended configuration.
- **TIES-Merging:** coefficient 0.3 as used in the original implementation.
- **TSV-M:** correction weight $\alpha = 1$, following the default configuration used in the official FusionBench implementation.

D. Ablation on Scaling Strategy: Beyond Simple Depth Priors

D.1. Comprehensive Comparison to Depth-Only Heuristics

In section 3.2.2 we discussed the tier-gate strategy that categorizes the layers and assign distinct scaling factors by the depth prior. To contextualize the proposed LARV scal-

Depth strategy			TIES	ISO-C	ISO-CTS	TSV-M
s_s	s_m	s_d				
Baseline						
1.0	1.0	1.0	71.9	82.5	82.7	83.1
Uniform						
0.5	0.5	0.5	64.6	74.6	74.8	77.6
1.5	1.5	1.5	72.7	81.3	81.2	78.2
Freeze Shallow Layers						
0.0	0.0	0.5	55.8	61.5	61.8	63.5
0.0	0.0	1.0	61.2	69.2	69.8	71.0
0.0	0.0	1.5	65.2	73.9	74.3	74.3
0.0	1.0	0.5	68.1	77.1	77.7	78.6
0.0	1.0	1.0	72.5	81.8	82.5	82.4
0.0	1.0	1.5	75.4	83.7	84.3	83.4
0.0	1.5	0.5	70.7	78.5	79.4	78.4
0.0	1.5	1.0	74.7	82.5	83.2	81.3
0.0	1.5	1.5	77.0	84.0	84.6	81.8
Freeze Deep Layers						
0.0	0.5	0.0	56.2	62.1	62.4	63.3
0.0	1.0	0.0	61.7	68.7	69.4	68.6
0.0	1.5	0.0	65.2	71.2	72.2	69.8
0.5	0.5	0.0	58.0	64.5	64.4	65.9
0.5	1.0	0.0	63.1	70.3	70.6	70.8
0.5	1.5	0.0	66.2	72.4	73.1	71.8
1.5	0.5	0.0	53.7	61.8	61.1	60.3
1.5	1.0	0.0	58.6	67.0	66.7	65.6
1.5	1.5	0.0	61.6	68.4	68.5	66.4

Table 6. Depth-only structural baselines across backbones on ViT-B/32. We use the same depth-scaling notation as Fig. 4, where s_s , s_m , and s_d denote the shallow-, middle-, and deep-layer scales, respectively. The first three columns list the specific (s_s, s_m, s_d) configuration, while the remaining columns report accuracy (no %) for four merge rules. *Uniform* sets all three tiers to the same scale; *Freeze Shallow* fixes $s_s = 0$ and varies (s_m, s_d); and *Freeze Deep* fixes $s_d = 0$ and varies (s_s, s_m).

ing rule, we compare it against several depth-only heuristics that assign fixed scale values based solely on layer index. Throughout this section, we use the unified notation s_s (shallow-layer scale), s_m (middle-layer scale), and s_d (deep-layer scale) to describe tiered schedules. These schedules do not rely on weight-derived signals such as e_ℓ or c_ℓ , and therefore represent purely structural depth priors.

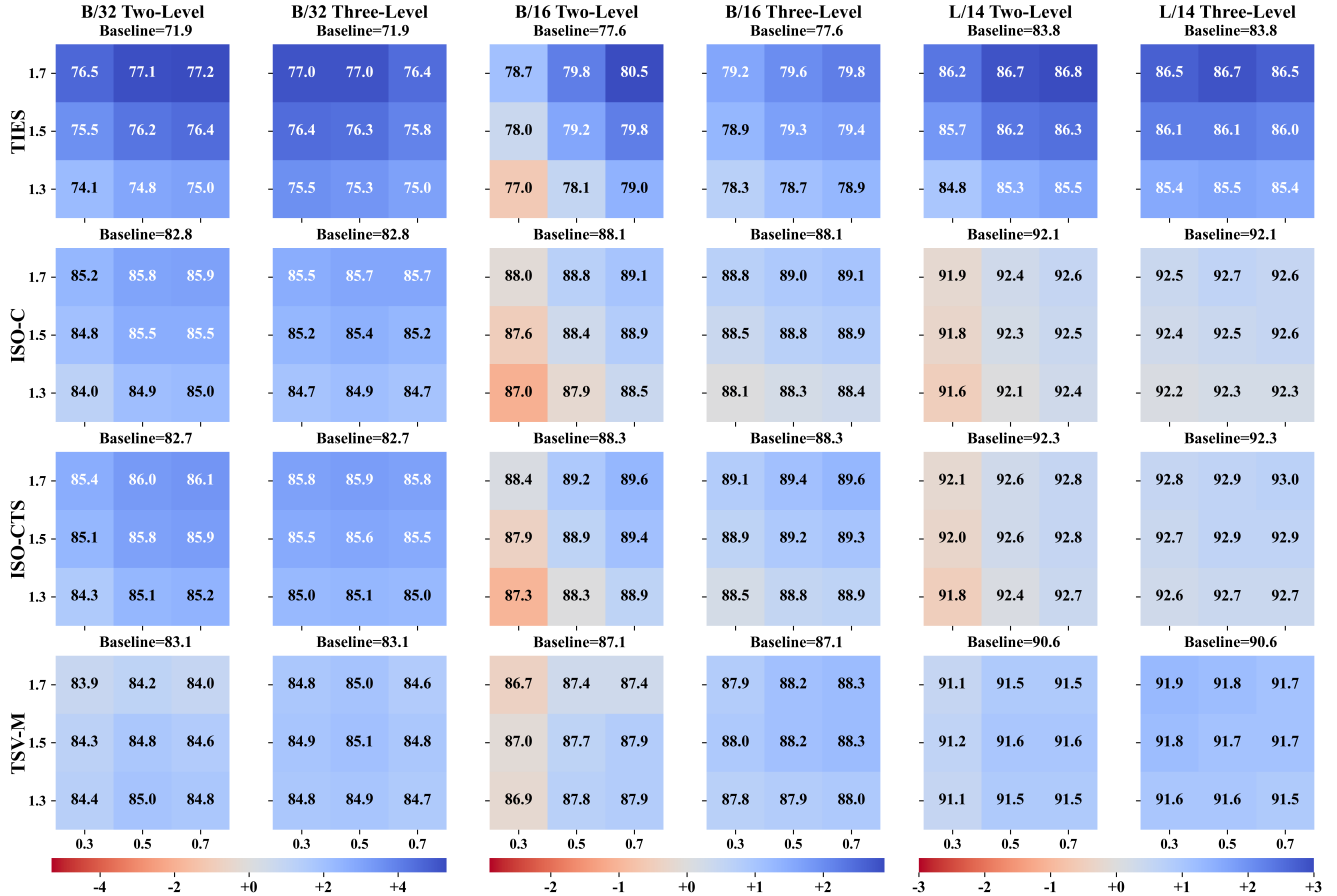


Figure 4. **Sensitivity of the tiered scaling scheme across eight vision tasks.** Each heatmap reports the Δ accuracy (LARV – Base, in percentage points) for a particular choice of tiered scaling coefficients. Positive values (red) indicate improvements, negative values (blue) indicate decreases, and the colormap is centered at zero so that color intensity reflects the magnitude of deviation from the baseline. The results show that moderate adjustments to middle or deep layers consistently provide the largest gains, highlighting the robustness of the tiered design across architectures.

Depth-only heuristics. We evaluate the following baseline strategies:

- **Uniform:** a single global scaling coefficient.
- **Tier2:** two-stage schedule with $s_s = 0.5$ for the shallow half and $s_d = 1.5$ for the deep half (with $s_m = 1$ implicitly).
- **Tier3:** three-stage monotonic schedule $(s_s, s_m, s_d) = (0.5, 1.0, 1.5)$.
- **Tier6:** six-stage coarse depth schedule $(0.5, 0.7, 0.9, 1.1, 1.3, 1.5)$.
- **Tier12:** fine-grained twelve-stage schedule increasing linearly from 0.5 to 1.5.
- **Linear:** continuous interpolation from $s_s = 0.5$ (shallow) to $s_d = 1.5$ (deep).

For backbones with different depths (e.g., ViT-B/32, ViT-B/16, ViT-L/14), this schedule is mapped proportionally across the L layers so that the relative progression remains

consistent. For comparison, we also include our full LARV scaling rule, which integrates the weight-derived EER and CCC signals into a composite score followed by a bounded nonlinearity. This strategy adapts the scaling value for each layer based on its learned behavior rather than its depth alone, and therefore departs fundamentally from depth-index heuristics.

Table 5 summarizes the 8-task average accuracy for four merging frameworks (TIES, ISO-C, ISO-CTS, TSV-M) on three ViT backbones (B/32, B/16, L/14). The results show that depth-only schedules—whether using uniform scaling, linear schemes, or multi-stage tiered splits—offer only mild and often inconsistent benefits when the backbone architecture changes. In comparison, LARV’s EER/CCC-guided layer-wise scaling improves all four merging methods on every backbone, suggesting that data-driven layer behavior provides a more stable and effective signal than simple

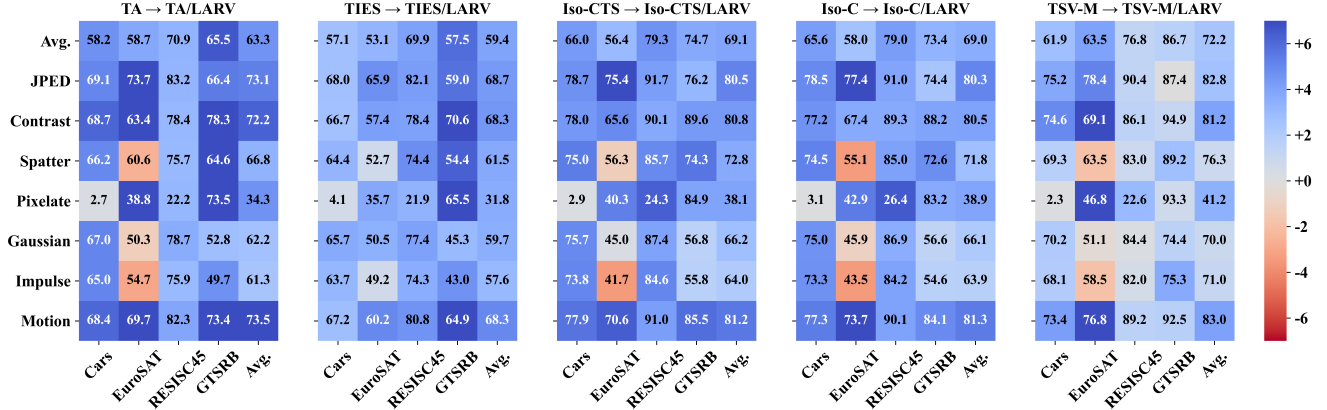


Figure 5. **Corruption-wise accuracy gains introduced by LARV.** Each heatmap visualizes the Δ accuracy (LARV – Base, in percentage points) across eight corruption types (Motion, Impulse, Gaussian, Pixelate, Spatter, Contrast, JPEG, and Avg.) evaluated on four datasets (Cars, EuroSAT, RESISC45, GTSRB) and their averaged performance. A positive delta indicates that LARV improves robustness, while a negative delta reflects a decrease in accuracy. The color map is centered at zero: red denotes negative changes, blue denotes positive improvements, and darker shades indicate larger magnitude.

depth-based heuristics.

D.2. Structural Analysis via Layer Freezing: Validating Depth Heterogeneity

To further analyze how different depth regions contribute to successful model merging, we conduct a series of depth-only structural ablations on ViT-B/32. These experiments freeze either the shallow layers or the deep layers, isolating how performance changes when specific portions of the network are prevented from adapting. The goal is not to propose new merging strategies, but to provide controlled evidence for the depth-dependent behavior observed throughout the main paper.

Experimental setup. We evaluate three families of depth configurations:

- **Uniform scaling:** all layers share the same scaling factor, such as (0.5, 0.5, 0.5), (1.0, 1.0, 1.0), and (1.5, 1.5, 1.5).
- **Freeze Shallow:** the shallow blocks are fixed (e.g., (0.0, ·, ·)), while the middle and deep layers remain scalable.
- **Freeze Deep:** the deep blocks are fixed (e.g., (·, ·, 0.0)), while earlier layers remain scalable.

These configurations represent deliberately extreme manipulations of depth. Unlike LARV’s three-stage scheme, which modulates shallow, middle, and deep layers smoothly, the freeze-based settings intentionally disrupt specific regions to reveal where useful semantic information resides.

Interpreting Table 6. Across all four merge rules, a consistent pattern emerges:

- **Freezing deep layers is the most harmful.** For every deep-frozen configuration, accuracy drops sharply (e.g., TIES: 56.2 → 61.6, ISO-C: 62.1 → 68.4), reflecting the loss of semantic alignment normally provided by the deepest blocks.
- **Freezing shallow layers results in much milder degradation.** Under shallow-freezing, performance remains relatively high (e.g., ISO-C reaches 84.0 and ISO-CTS reaches 84.6), indicating that early layers largely encode task-specific or noisy variations that are less critical for successful merging.
- **Both extremes underperform uniform scaling.** Even the best freeze-based results fall short of uniform configurations such as (1.0, 1.0, 1.0), highlighting that neither the shallow nor the deep region can be removed from adaptation without cost.

These structural ablations confirm the core motivation behind the three-stage depth-aware scaling strategy. Shallow layers tend to be noisy and should not dominate the merge; deep layers carry the strongest task-invariant semantics and must be scaled more aggressively; and the middle region acts as a stabilizing transition. By smoothly adjusting scaling across depth rather than freezing or treating all layers equally, LARV preserves the strengths of each depth region and produces more robust merged models.

D.3. Tiered Scaling Robustness and Sensitivity Analysis

Figure 4 provides a detailed sensitivity analysis of the two-level and three-level tiered scaling schemes across eight vision tasks and three ViT backbones (B/32, B/16, L/14). Several consistent and architecture-invariant patterns emerge.

First, **deep-layer amplification (s_d) is universally beneficial**. For all merging rules (TIES, Iso-C, Iso-CTS, TSV-M), increasing s_d from 1.0 to 1.5 yields monotonic gains, particularly on B/32 and B/16. This trend aligns with our diagnostic metrics: deeper blocks exhibit higher information richness (e_ℓ) and lower conflict (c_ℓ), so amplifying their contributions reliably strengthens semantic alignment across tasks.

Second, **shallow-layer shrinkage (s_s) consistently prevents degradation**. Across all backbones, settings with $s_s = 0.5$ outperform or match $s_s = 1.0$, while aggressive amplification ($s_s = 1.5$) frequently harms performance—especially for TIES and ISO-C on B/32. This supports our central hypothesis that early layers contain noisy or task-specific variations that should not be emphasized during merging.

Third, **three-level schemes offer smoother, more stable behavior**. While two-level schedules already outperform uniform scaling, the three-level variant reduces performance variance by adding a flexible middle tier (s_m). This middle bucket prevents over-shrinkage or over-amplification, leading to more robust cross-rule improvements. The effect is particularly visible on Iso-CTS and TSV-M, where most (s_s, s_m, s_d) configurations form a flat plateau of strong results around (0.5, 1.0, 1.5).

Finally, **scaling trends persist across backbones and merging rules**, demonstrating that layer-wise heterogeneity is a structural, architecture-agnostic property of ViTs rather than an artifact of a specific rule or dataset. Larger backbones (e.g., ViT-L/14) show slightly reduced sensitivity overall, suggesting that increased capacity mitigates interference but still benefits from depth-aware scaling.

Overall, the sensitivity maps reinforce the design of LARV’s tiered scaling: suppress noisy shallow updates, stabilize mid-depth transitions, and amplify deep semantic structure. This explains why LARV remains effective across merge rules and backbones despite using a fixed, data-free policy.

E. Full Results on Robustness and Generalization

E.1. Detailed Results on Corruption Tasks

In the main paper, we use radar plots to summarize each method’s robustness trend across corruption types, providing a high-level comparison of the baseline mergers and their LARV-enhanced variants. While these visualizations reveal the overall shape of performance differences, they do not expose the fine-grained behavior of each dataset under specific corruption settings.

To provide a complete picture, this section reports the full corruption-wise performance details. Instead of repeating raw accuracies, we visualize the Δ accuracy (LARV – Base, in percentage points) for all eight corruption types across the

four datasets and their averaged performance. This representation makes the effect of LARV immediately interpretable: positive Δ values indicate robustness improvements, negative values indicate decreases, and the diverging colormap centers zero to highlight the direction and magnitude of change.

These detailed heatmaps reveal several patterns that complement the aggregated observations in the main text. LARV consistently improves robustness across most corruptions and methods, but the gains are not uniform. High-frequency distortions such as Pixelate, Spatter, and Contrast show particularly large improvements, suggesting that LARV stabilizes deeper transformer blocks that are especially sensitive to such perturbations. Even when baseline performance is strong, LARV provides additional robustness headroom without degrading accuracy on simpler corruptions.

Overall, these detailed results corroborate the conclusions drawn from the radar plots: LARV yields systematic, architecture-agnostic robustness gains and provides a more reliable corruption response profile across merging methods.

E.2. Generalization Beyond Vision

To assess modality generality, we evaluate LARV on NLP tasks using T5-LoRA adapters across eight language tasks. Without any re-tuning, LARV consistently improves all base merging rules, indicating that layer-wise interference patterns and weight-only diagnostics extend beyond vision transformers. Detailed results are provided in the Appendix.

E.3. Detailed Results on 14-Task and 20-Task Merges

Tables 7 and 8 provide the complete accuracy results for the 14-task and 20-task merging benchmarks, complementing the aggregated performance curves shown in the main paper. While the main text focuses on overall improvements and backbone-level trends, the full tables reveal several deeper insights into how LARV behaves across tasks, architectures, and merge rules.

First, LARV produces improvements that are surprisingly stable across both the 14-task and 20-task settings, despite the substantial increase in task diversity. Moving from 14 to 20 tasks introduces broader variations in granularity (e.g., GTSRB vs. Food101), modality shift (e.g., PCAM and FER2013), and texture-heavy domains (e.g., DTD). Traditional merge baselines struggle in such heterogeneous settings because scaling errors propagate unevenly across layers; LARV counteracts this by rebalancing shallow, middle, and deep representations in a task-agnostic way, enabling consistent gains even when the underlying task mixture becomes more challenging.

Second, the tables highlight that LARV’s benefits are not uniform but follow an interpretable pattern aligned with

Method	LARV	SUN397	Cars	RESISC45	EuroSAT	SVHN	GTSRB	MNIST	DTD	Flowers	PCAM	FER2013	Pets	STL10	CIFAR100	Avg.
ViT-B/32																
Fine-tuned	-	82.8	92.8	97.4	99.1	97.9	99.2	99.8	85.5	97.7	91.1	75.9	95.8	99.2	93.0	93.4
Simple Avg.	-	64.8	60.4	67.1	67.0	50.7	45.6	76.6	46.9	67.4	65.2	51.6	84.2	97.2	70.4	65.4
Task Arithmetic	-	41.8	33.2	47.3	55.4	46.5	48.4	88.7	37.0	38.6	64.1	46.1	65.9	84.6	41.7	52.8
	✓	51.1	44.4	60.0	82.6	68.3	65.9	96.3	46.1	50.0	70.1	57.3	76.8	93.5	59.2	65.8↑
ISO-C	-	69.5	62.6	79.8	83.4	78.4	84.1	97.0	61.2	69.3	83.6	65.6	87.1	96.8	74.3	78.1
	✓	72.1	63.0	87.4	91.2	77.7	87.7	97.7	68.9	73.5	82.2	68.4	88.5	97.8	80.2	81.2↑
ISO-CTS	-	69.7	68.0	81.6	85.3	78.1	85.7	97.5	62.9	73.5	84.6	67.1	87.0	97.0	74.2	79.4
	✓	72.2	69.5	89.4	91.4	77.0	88.7	97.8	71.4	79.8	81.4	69.1	87.6	97.9	80.7	82.4 ↑
TIES	-	62.2	54.6	65.3	63.0	65.7	63.9	92.6	49.9	58.2	77.1	54.9	81.4	94.8	62.4	67.6
	✓	63.3	56.7	74.4	83.3	75.9	73.9	96.3	54.3	61.7	76.6	61.9	83.0	97.0	72.1	73.6↑
TSV-M	-	66.5	62.6	80.7	91.3	86.7	89.3	98.6	60.9	66.2	81.3	65.3	87.4	96.7	69.5	78.8
	✓	67.4	63.3	85.8	94.7	86.0	90.8	98.7	67.8	72.2	80.5	68.2	89.0	97.8	74.9	81.2↑
ViT-B/16																
Fine-tuned	-	78.9	85.9	96.6	99.0	97.6	99.0	99.7	82.3	94.9	90.6	72.8	94.5	98.2	88.8	91.3
Simple Avg.	-	67.5	65.9	71.5	71.1	64.6	54.1	82.6	47.2	72.5	63.2	54.1	90.4	98.3	73.4	69.7
Task Arithmetic	-	52.5	40.8	52.0	50.5	59.4	50.7	90.1	37.1	49.8	82.4	55.6	87.2	92.8	50.0	60.8
	✓	62.4	49.0	73.8	79.9	77.2	71.5	97.2	45.7	63.6	82.9	65.1	92.4	96.7	68.8	73.3↑
ISO-C	-	72.8	66.2	88.2	91.8	86.7	87.7	98.2	60.1	81.0	82.6	67.0	93.9	98.4	79.5	82.4
	✓	74.4	63.0	91.3	95.7	86.0	89.3	98.4	68.7	86.1	82.4	70.1	94.0	98.9	82.7	84.3↑
ISO-CTS	-	73.5	74.1	90.1	94.3	89.0	90.4	98.3	65.3	85.5	81.2	68.6	93.8	98.5	80.0	84.5
	✓	74.9	72.9	92.5	96.2	87.3	90.9	98.5	73.7	91.0	82.1	70.9	93.7	98.9	82.5	86.1 ↑
TIES	-	66.9	60.3	71.9	69.8	71.4	64.4	93.6	49.0	64.8	73.1	59.6	90.8	97.6	67.9	71.5
	✓	69.4	60.7	82.1	84.9	78.4	77.1	96.9	54.1	70.6	71.8	67.2	93.3	98.3	77.5	77.3↑
TSV-M	-	70.1	66.9	85.6	92.6	88.7	88.4	98.7	59.3	77.5	84.4	69.7	93.6	98.0	76.3	82.1
	✓	71.8	67.1	89.7	96.2	88.4	90.5	98.9	66.4	83.9	82.8	70.8	94.1	98.5	80.0	84.2↑
ViT-L/14																
Fine-tuned	-	74.9	78.5	95.1	99.1	97.3	98.9	99.6	79.7	88.6	88.0	71.6	92.5	97.6	88.4	89.3
Simple Avg.	-	71.2	79.0	78.7	80.4	71.3	64.6	94.3	58.7	81.9	74.2	54.8	94.6	99.3	82.4	77.5
Task Arithmetic	-	60.6	53.2	48.1	53.0	50.1	54.2	93.0	41.6	59.6	75.8	53.9	89.3	94.2	57.2	63.1
	✓	68.5	68.6	70.7	77.6	77.1	72.1	97.7	53.6	77.9	78.5	60.8	93.3	98.2	74.0	76.3↑
ISO-C	-	78.9	89.1	93.8	94.5	91.8	94.8	98.8	74.4	96.7	85.8	70.9	96.6	99.6	87.7	89.5
	✓	80.2	90.4	94.8	96.8	90.6	94.7	98.9	79.0	97.8	85.1	73.5	96.5	99.5	89.6	90.5↑
ISO-CTS	-	79.8	90.7	94.8	95.9	92.6	95.9	99.0	78.0	97.4	84.1	72.8	96.6	99.6	88.4	90.4
	✓	80.6	91.8	95.7	97.4	91.1	95.6	98.9	81.4	98.0	84.6	74.3	96.3	99.5	89.6	91.1 ↑
TIES	-	72.0	75.6	76.5	69.7	77.2	75.1	96.6	57.8	79.6	78.2	60.0	94.7	98.4	77.7	77.8
	✓	74.3	80.7	84.9	89.1	84.5	83.0	98.2	63.6	87.2	83.1	64.7	95.4	99.1	84.5	83.7↑
TSV-M	-	76.0	86.7	91.1	94.2	93.2	93.8	99.0	69.5	95.1	86.0	69.8	96.3	99.2	85.2	88.2
	✓	77.8	89.1	93.0	97.3	92.8	94.4	99.0	76.1	97.1	84.2	72.9	96.3	99.3	87.7	89.8↑

Table 7. Results on 14 classification tasks across five ViT backbones. For each backbone (ViT-B/32, ViT-B/16, ViT-L/14), we report the accuracy (%) of seven merging methods, with and without LARV. Fine-tuned models are included as an upper bound. Best results per task (excluding Fine-tuned) are highlighted in bold. This table complements the high-level robustness trends shown in the main paper by providing per-dataset accuracy details, demonstrating that LARV consistently improves or matches performance across diverse tasks and architectures.

	LARV	TA	ISO-C	ISO-CTS	TIES	TSV-M
TS-LoRA	-	77.41	76.28	76.26	76.79	81.83
TS-LoRA	✓	78.00↑	76.44↑	76.43↑	77.52↑	82.21↑

Table 8. Additional Experiments on 8 NLP Tasks.

the analysis in the main paper. Fine-grained and structure-dependent datasets (Cars, Pet Images, Flowers102, STL10, CIFAR100) tend to benefit the most. These tasks rely heavily on spatially precise or high-frequency cues, which are sensitive to mismatched feature magnitudes after merging. LARV’s adaptive depthwise rescaling helps recover these signals, especially in deeper layers where semantic abstraction is formed. Conversely, tasks with extremely low intrinsic dimensionality (e.g., MNIST, KMNIST) exhibit smaller but still positive gains, consistent with the idea that early transformer blocks dominate their decision boundaries.

Third, cross-backbone consistency offers additional ev-

idence that the LARV mechanism generalizes beyond any particular model scale. ViT-B/32 gains are the largest in relative terms, reflecting that coarse-grained early representations are particularly vulnerable to scaling mismatch. In contrast, ViT-L/14—whose deeper feature hierarchy already exhibits stable layer statistics—still benefits from LARV, but the improvements manifest more in robustness across tasks than in raw accuracy. This agrees with our findings in §4 that deeper backbones exhibit smaller variance in their layer-wise magnitudes, yet still profit from controlled rescaling at block level.

Finally, the detailed results also reveal systematic differences between merge rules. Methods with inherently stronger geometric alignment (ISO-C, ISO-CTS) tend to show more moderate but still consistent gains under LARV, whereas magnitude-sensitive mergers (TIES, TSV-M) show the largest absolute improvements. This pattern aligns with the theory that LARV corrects scaling distortions that ac-

accumulate during magnitude-based merging, especially in deeper layers. Importantly, LARV never degrades performance in a systematic way, demonstrating that its veneer formulation serves as a reliable drop-in enhancement to a wide range of merging templates.

Overall, the complete results in Tables 7 and 8 substantiate the main claim of the paper: LARV improves multi-task model merging not simply through uniform rescaling, but through a principled depth-aware correction that stabilizes representations across a wide spectrum of datasets, architectures, and merging paradigms.

